Plasmon-Enhanced Spectral Changes in Surface Sum-Frequency Generation with Polychromatic Light

by

Luyu Wang

Submitted in partial fulfilment of the requirements
for the degree of Master of Applied Science

at

Dalhousie University
Halifax, Nova Scotia
August 2013

献给我的父母。

To my parents.

TABLE OF CONTENTS

LIST OF FIGURES

ABSTRACT

In this thesis, the spectral behavior of the fundamental and sum-frequency waves, generated from the surface of a thin metal film in the Kretschmann configuration, is theoretically studied with coherent ultrashort pulses. As a first exploration of considering spectral response in nonlinear plasmonics, it is shown that the spectra of reflected sum-frequency waves exhibit pronounced shifts for the incident fundamental waves close to the plasmon coupling angle, whereas meanwhile those of reflected fundamental waves display energy holes. We also demonstrate that the scale of discovered plasmon-enhanced spectral changes is strongly influenced by the magnitude of the incidentce angle and the source pulse duration, and at a certain angle a spectral switch is observed. The appearance of large sum-frequency wave shifts can serve as an unambiguous plasmon signatur in nonlinear surface spectroscopy. Also, the discovered spectral switch can trigger extremely surface-sensitive nonlinear plasmonic sensors.

LIST OF ABBREVIATIONS AND SYMBOLS USED

ATR	Attenuated Total Reflection
CCD	Charged-Coupled Device
DFG	Difference-Frequency Generation
FW	Fundamental Wave
NLO	Nonlinear Optics
SFG	Sum-Frequency Generation
SFW	Sum-Frequency Wave
SHG	Second-Harmonic Generation
SPP	Surface Plasmon Polariton
SPR	Surface Plasmon Resonance
ε	Permittivity
ω	Angular frequency
ε'	Real part of a complex permittivity
ε''	Imaginary part of a complex permittivity
k	Wavevector
k'	Real part of a complex wavevector
k''	Imaginary part of a complex wavevector
k_x	Tangential component of a wavevector
θ_i	Angle of incidence
n	Refractive index
c	Speed of light in vacuum
$\chi^{(1)}$	Linear electric susceptibility
ε_0	Free space permittivity
$\chi^{(2)}$	Second-order nonlinear electric susceptibility
$\mathbf{e}_i$	Unit vector in i-direction
A	Electric field amplitude
k_z	Normal component of a wavevector
μ_0	Free space permeability
S	Energy spectrum
r_{ij}	Fresnel reflection coefficient
λ	Wavelength
t_{ij}	Fresnel transmission coefficient
P_0	Polarization amplitude
G_{ij}	Dyadic Green's function tensor
G_0	Scalar free-space Green's function
δ_{ij}	Dirac function
ω_p	Plasma frequency
Γ	Damping rate
ω_0	Bound electron resonant frequency
n_B	Equilibrium free-electrom density in the bulk
e	Electric charge of an electron
θ_c	Plasmon coupling angle
t_p	Laser pulse duration

ACKNOWLEDGEMENTS

I would like to express my sincere gratitude to my supervisor Dr. Sergey Ponomarenko, who has shared not only part of his immense knowledge with me, but also the science spirit that will surely benefit me till the end of my life. Without his guidance and help, it is impossible for me to finish my research and to write this thesis.

I really appreciate the help of my co-supervisor, Dr. Zhizhang Chen, for his support during my studies, and for quite a few conversations full of insightful thoughts.

It is a pleasure working with the groupmates in both Dr. Ponomarenko's and Dr. Chen's group. Many thanks to the kind help of Mr. Franklin Che and Ms. Laleh Mokhtarpour.

Meanwhile, I would like to thank the rest of my thesis committee: Dr. Yuan Ma and Dr. William Philips, for reading the thesis, and their useful comments and recommendations.

Finally, my sincere love goes to my family: my parents Wang Bin and Guo Dongmei.

CHAPTER 1 INTRODUCTION

1.1 BACKGROUD

Since the inception of the electromagnetic theory, we have witnessed enormous progress of how the newly invented tools could continue our incomplete biological evolution. To name a few, circuit theory, a simplified and practical version of Maxwell's equations, triggered some of our greatest inventions – electronics and the computer; making use of electromagnetic energy allows us to communicate with people even on the other side of our planet, through radio or microwaves; we can also interact with the molecular or atomic world easier – by firing scary high-power laser beams onto the matter, and seeing what will happen. All these advances that we couldn't imagine as hungry cavemen, remarkably extend the outreach of our brains and hands, cultivating a vivid society that is progressing to an even more advanced and sophisticated one.

Nowadays, electromagnetism seems to be too mature to provide us with anything new. Yet based on exactly the same Maxwell equations and some particular boundary conditions, the emerging area of *plasmonics* has been growing rapidly since the first decade of the twenty-first century [1]. Origining from interaction processes between electromagnetic radiation and conduction electrons at metallic interfaces or in small metallic nanostructures, the so-called Surface Plasmon Polaritons (SPPs) leads to an enhanced optical near field of sub-wavelength dimension. It can break the diffraction limit of light in free space, and thus can be used to reduce the physical size of an ultrafast photonic device [2]. When the external electromagnetic energy oscillates resonantly with SPPs, the extreme surface sensitivity of surface plasmon resonance (SPR) also becomes invaluable in surface chemical studies [3]. Besides, the area of plasmonics, young but rich in phenomena, has found more applications including much faster computer chips (into the 100 THz range) [4], high-resolution lithography and microscopy [5], organic light-emitting diodes [6], national security/environmental monitoring [7], medical drag delivery [8], full color holograms [9], and photovoltaic cells [10].

1.2 MOTIVATION

The existence of SPPs, special surface electromagnetic modes that are confined to a surface, was predicted by Sommerfield in 1909 [11]. It requires a medium with a negative optical dielectric constant, and metal films at frequencies sufficiently below the plasma frequency can serve to this end. In particular, Kretschmann configuration has been used extensively because of its simplicity and efficiency in SPPs excitation [12]. However, much research deals with only *linear* light-matter interaction modalities [3, 13]. Due to the strong field enhancement on the metal surface, the area of *nonlinear* optics naturally called for its extension to the SPPs. Second-harmonic generation (SHG) by SPPs was first observed by Simon *et al*. [14], followed by other wave mixing processes involving SPPs [15, 16]. Nevertheless, majority of the work in plasmonics has been focused on quasi-monochromatic light. In reality, even the line spectrum of a laser beam has a finite bandwidth. Those with wideband spectra could be rich in spectral signatures of plasmon enhanced electromagnetic fields. Recently, the linear optical response of different plasmonic nanostructures probed with broadband light laser beams has been studied [17, 18]. However, to the best of the author's knowledge, plasmon-enhanced nonlinear optical processes with polychromatic light sources have not been examined yet. It is very instructive to know whether plasmons will leave any spectral signatures in the far-field of generated second-order nonlinear waves or not. If the answer is in the affirmative, this could make new developments possible in surface nonlinear spectroscopy, microscopy, and surface morphology studies.

1.3 THESIS CONTRIBUTIONS

This thesis presents the first exploration of spectral response in nonlinear plasmonics. In this work, we have made the following contributions:

- We investigated the spectral behavior of the fundamental and sum-frequency waves in the surface sum-frequency generation (SFG) from a thin gold film with polychromatic incident light.

- We found that at the incidence angle corresponding to light coupling to the surface plasmon, the spectral behaviors of reflected fundamental and sum-frequency waves (SFW) are totally different: the former has a spectral hole at the carrier frequency whereas the spectrum of the latter gets blue-shifted from the expected maximum. The appearance of large SFW shifts can serve as an unambiguous plasmon signature in nonlinear surface spectroscopy. Also, as the incidence angle deviates from the plasmon coupling angle, all spectral changes disappear.
- We found that the shifts of SFW spectra become more pronounced as the source bandwidth increases. This could be useful when trying to control the shifts with tunable lasers.
- Finally, we found that at a certain angle a nonlinear spectral switch is observed, which could help advance conventional linear plasmonic sensors into a much higher accuracy level.

In general, the results may make new developments possible in surface nonlinear spectroscopy, microscopy, surface plasmon sensing, and surface morphology studies.

1.4 Thesis Organization

The remainder of the thesis is organized as follows. Chapter 2 is a review of foundations of following theoretical work – including an introduction to SPPs, a couple of optical coupling methods, and the concept of polychromatic light. Chapter 3 presents the derivations of the theory, and later the results and discussions. Finally, conclusions and recommendations are pointed out in Chapter 4.

CHAPTER 2 BACKGROUND INFORMATION

2.1 INTRODUCTION TO PLASMONICS

An emerging branch of optical physics is plasmonics which is now experiencing a truly explosive growth in popularity. It requires an evanescent electromagnetic surface wave to excite SPPs by light, which exists on an interface between a medium with a negative optical dielectric constant and another medium with a positive one (Fig. 2.1). To efficiently excite SPPs, different optical coupling methods have been developed. When the free electrons of metal respond collectively by oscillating in resonance with external light wave, surface plasmon resonance (SPR) occurs. Combining SPPs and nano-optics, plasmonics is a cutting-eage technology that squeezes light into diminutive structures. It may yield, for example, a new generation of ultrafast computer chips and supersensitive molecular detectors.

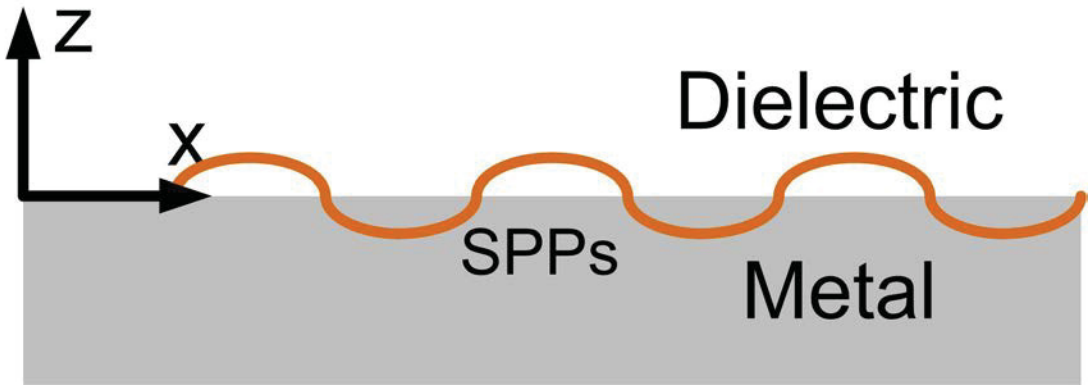

Figure 2.1 Geometry for SPP propagation at a single interface between a metal and a dielectric.

2.1.1 Surface Plasmon Polaritons

SPPs can exist on a geometry as simple as a surface (Fig. 2.1) separating two nonmagnetic media: a dielectric with positive real dielectric constant ε_d and an adjacent

medium described via a complex dielectric function $\varepsilon_m(\omega)$, where ω is the angular frequency (we write $\varepsilon_m(\omega)$ as ε_m hereafter for concision). It is required that $\mathrm{Re}[\varepsilon_m(\omega)] < 0$, while in optical regime metal can serve to this end [1, Chap. 1]. Solving the Maxwell equations with boundary conditions in the media gives us the dispersion relation of a SPP [1, Chap. 2]

$$k_{spp} = \frac{\omega}{c}\sqrt{\frac{\varepsilon_m \varepsilon_d}{\varepsilon_m + \varepsilon_d}} \tag{2.1}$$

where c is the speed of light in vacuum.

If we assume that $\varepsilon_m = \varepsilon'_m + i\varepsilon''_m$ and $k_{spp} = k'_{spp} + ik''_{spp}$, in the case that $\varepsilon'_m < 0$, $\left|\varepsilon'_m\right| >> \varepsilon''_m$, the real and imaginary parts of the SPP wave number are

$$k'_{spp} = \frac{\omega}{c}\sqrt{\frac{\varepsilon'_m \varepsilon_d}{\varepsilon'_m + \varepsilon_d}}, \tag{2.2}$$

$$k''_{spp} = \frac{\omega}{c}\left(\frac{\varepsilon'_m \varepsilon_d}{\varepsilon'_m + \varepsilon_d}\right)^{\frac{3}{2}} \frac{\varepsilon''}{2\left(\varepsilon'_m\right)^2}. \tag{2.3}$$

It is concluded from Eq. (2.2) that k'_{spp} is real, indicating the SPP mode can propagate along the interface. The exsistance of k''_{spp} results in large losses during propagation, limiting the transmission range of such a mode – this problem has drawn lots of attentions particularly in the design of plasmonic waveguides [1, Chap. 7].

Either light [12, 19] or electrons [20] can excite SPPs. When light is incident at an angle of θ through a medium of refractive index n_1, SPPs can be exited as satisfying the linear momentum conservation along the surface, i.e.,

$$k_x = k\sin\theta = k'_{spp} \tag{2.4}$$

where $k = n_1 \omega / c$ is the wave number of light in the dielectric. The dispersion relations of SPPs and of light are plotted in Fig. 2.2, which are excited on a metal/air interface [21]. It can be seen in the figure that the dispersion curve of SPPs bends – at a same frequency, SPP has a larger wavevector k_x than that of light in free space – the physical reason is that the light field has to "drag" energy from electrons along the metal surface. As a consequence, a SPP on such an interface cannot be excited by light of any frequency propagating in air. Translating into dispersion relations in Fig. 2.2, the curve of SPPs is always on the right side of the light curve. In fact, only if the two curves cross can SPPs be excited. With regards to this, an efficient optical coupling method is demanded.

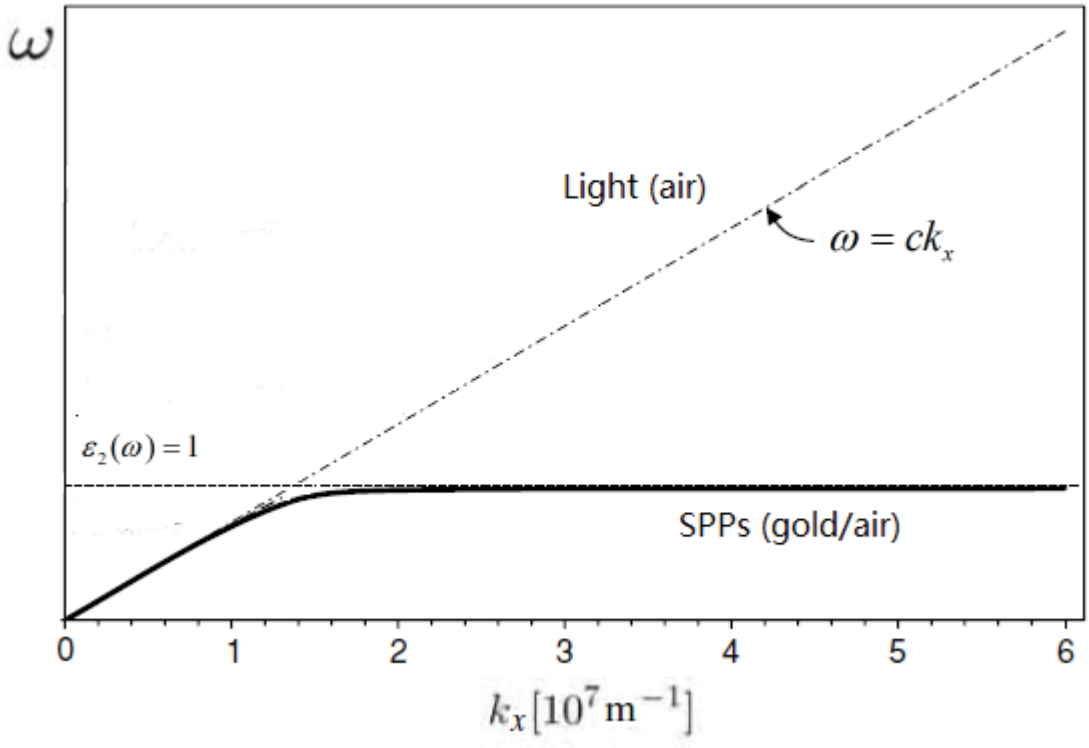

Figure 2.2 Dispersion relation of SPPs at a gold/air interface. The solid line is the dispersion relation that results from a dielectric function accounting for a single interband transition. The dash-dotted straight line is the light line $\omega = ck_x$ in air (Figure source: Fig.12.5, pp. 388, [21]).

2.1.2 Optical Coupling Methods

Glass provides a larger refractive index than does air, which has been proven useful to increase the wavevector component k_x of the exciting light over its free-space value. To this end, the Otto configuration [19] and Kretschmann configuration [12] have been proposed, as displayed in Fig. 2.3. Both configurations make use of the prism coupling. In the Otto configuration [Fig. 2.3(a)], metal and glass are separated by an air gap of the order of wavelength. Light energy tunnels through the tail of evanescent waves to the metal layer and therefore SPPs can be excited on the air/metal interface. But experimentally it is extremely hard to control such a small gap between prism and thin film. The Kretschmann configuration [Fig. 2.3(b)] then comes to rescue – a thin metal film of tens of nanometers is coated directly on the prism. Due to its simplicity and high stability, the Kretschmann configuration is considered to be the most popular configuration in SPR experiments. In this thesis, we are going to theoretically study the nonlinear SPP generation in this kind of configuration as well.

By using such configurations, SPPs can be efficiently excited on the metal/air interface. Fig. 2.3(c) displays the dispersion curve of light in a glass, on right of that in air, making a crosspoint with the curve of SPPs at the gold/air interface: it corresponds to the maximum SPP generation frequency. Thus, changing the incidence angle θ properly can allow for k_x satisfy relation (2.4), and the incident light energy can then be efficiently coupled to SPPs. Researchers usually measure the reflectivity curves in the Kretschmann configuration [13]. The occurrence of a minimum in such curves at a particular incidence angle θ has a physical interpretation as: the missing light has been totally converted to SPPs localized at the interface and cannot be reflected to the detector in the far-field. Under this condition, the free electrons of metal oscillate collectively and in resonance with the incident light. This phenomenon is also termed as "surface plasmon resonance (SPR)", which has found numerous applications in chemical and biological sensor applications (for a review article of SPR sensors see Ref. [3]).

Except for the prism coupling, alternative ways to excite SPPs include grating coupling, highly focused optical beams, near-field excitation, and so on [1, Chap. 3].

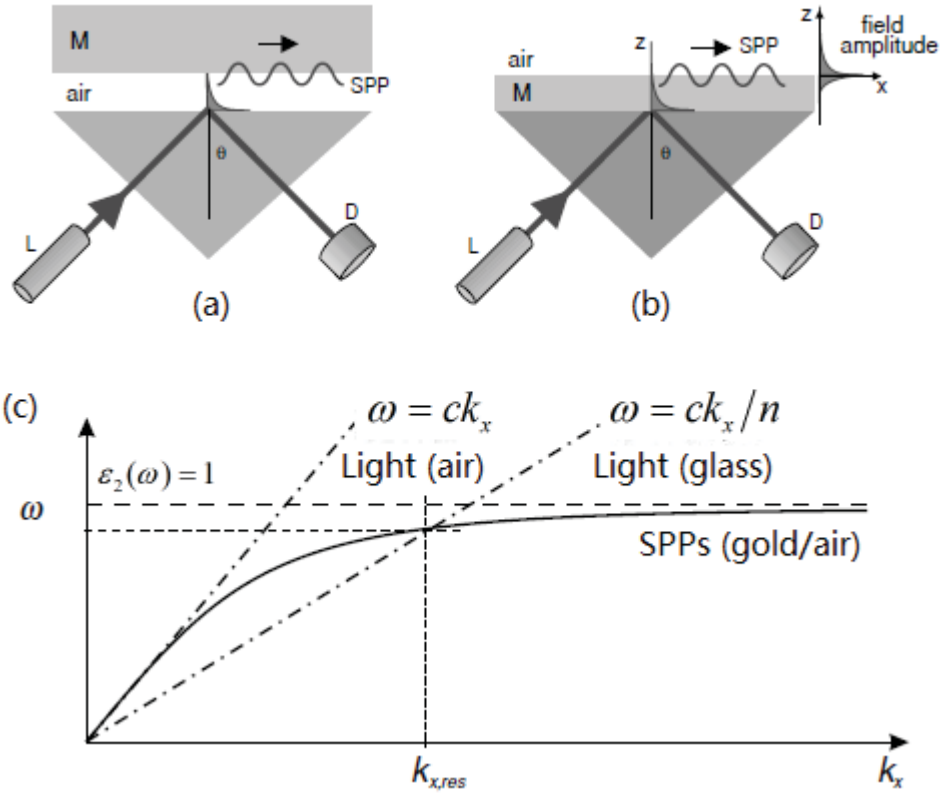

Figure 2.3 Excitation of surface plasmons in the (a) Otto configuration and (b) Kretschmann configuration. L: laser, D: detector, M: metal layer. Both of them are the experimental arrangements to realize the condition sketched in (c): close-up of the dispersion relation with the free-space light line and the tilted light line in glass. (figure source: Fig. 12.6, pp. 389, [21]).

2.1.3 Plasmonics

Plasmonics is a crosspoint of SPPs and nano-optics. The term was coined by the research group at California Institute of Technology in 2000. The next decade witnessed an explosive growth and numerous research papers [22-24], review articles [4, 25-28]. Researchers have explored this area into various kinds of advanced applications, including fabrication of sub-wavelength optical devices and chips [25-27], merging photonics and electronics at nanoscale dimensions [2], destroying cancer tumors [4], and designing invisibility cloak [4]. Nowadays electronic devices have reached their physical limitations, but optical devices can support systems 1000 times faster than those

employing electronic devices. Nevertheless, the sizes of photonic components are usually in the order of micrometers, whereas electronics has reached as small as the nano-scale. The sizes of photonics devices are limited by the so-called "diffraction limit" [29], exceeding which will result in prohibitively large diffraction, making them impossible to operate.

Plasmonic technology can help us close this gap between photonics and electronics: now it is possible to design photonic devices dramatically smaller in size, by squeezing light into a subwavelength scale. Thus, plasmonics is promising to merge photonics and electronics in the nano-world, fast and small [2]. With that we may be able to develop ultrafast plasmonic computers which could be thousands times faster than modern personal computers [4].

2.2 Second-Order Nonlinear Processes

An important study in optics is to investigate, by the presence of light, what the modification of the optical properties of a material system will result in. Majority of the work was focusing on only linear optics till shortly after the ruby laser was invented [30] – when the second harmonic generation was discovered in quartz crystals by Franken *et al*. in 1961 [31]. Nonlinear optics (NLO), the first and the largest field created by the invention of laser, is a branch of optics that studies the behavior of light in nonlinear media, i.e., media in which the dielectric polarization **P** responds nonlinearly to the electric field **E** of the light [32]. This kind of nonlinearity typically can only be observed at very high input light field intensities (typically 10^8 V/m) such as those provided by pulsed lasers. Hence, it has been providing us with not only interesting basic physics, but also useful applications. In recent years, the subfield of surface nonlinear optics has drawn more and more attentions. Nonlinear optical techniques developed as surface probes have been proven powerful in the area of surface science [3, 33]. Meanwhile, the explosive-growing area of plasmonics has called for the extension to nonlinear optics – nonlinear plasmonics holds promises for the future optical technology development [34].

2.2.1 Theory

When the matter is placed in an external field, its atoms or molecules can be induced or reoriented with dipole moments – the matter polarization is produced. Polarization is described in terms of a polarization field **P** which is a dipole moment per unit volume at a given source point within the matter. The latter is proportional to the field strength, if the applied electric field is not too large [32]:

$$P = \varepsilon_0 \chi^{(1)} E \,, \tag{2.5}$$

where $\chi^{(1)}$ is the usual susceptibility in linear optics. Note that Eq. (2.5) is written in a scalar format for simplicity.

With the invention of modern high-power lasers, Eq. (2.5) no longer holds, as the nonlinear response begins to play a role. Under this condition, electron displacements can occur and add additional contributions to the polarization such that

$$P = \varepsilon_0 \left(\chi^{(1)} E + \chi^{(2)} E^2 + \chi^{(3)} E^3 + ... \right), \tag{2.6}$$

where the superscript "2" and "3" correspond to the second- and third-order susceptibilities, respectively.

We now qualitatively look into second-order processes, which are the strongest and easiest to detect nonlinear processes. To start with, consider an input field with two different input frequencies ω_1 and ω_2,

$$E(t) = \frac{1}{2}\left(\mathrm{E}_1 e^{-i\omega_1 t} + \mathrm{E}_2 e^{-i\omega_2 t} + c.c \right), \tag{2.7}$$

The generated output polarization can be represented as

$$P^{(2)}(t) = \frac{1}{2} \sum\nolimits_s \mathrm{P}\left(\omega_s \right) e^{-i\omega_s t} + c.c \,, \tag{2.8}$$

where the summation is over all possible combinations of two frequency components. Its elements are found to be

$$\mathrm{P}_{SHG}(2\omega_j) = \frac{1}{2}\varepsilon_0 \chi^{(2)} \mathrm{E}_j^2, \tag{2.9}$$

$$\mathrm{P}_{SFG}(\omega_1 + \omega_2) = \varepsilon_0 \chi^{(2)} \mathrm{E}_1 \mathrm{E}_2, \tag{2.10}$$

$$\mathrm{P}_{DFG}(\omega_1 - \omega_2) = \varepsilon_0 \chi^{(2)} \mathrm{E}_1 \mathrm{E}_2^*, \tag{2.11}$$

$$\mathrm{P}_{OR}(0) = \varepsilon_0 \chi^{(2)} \left(|\mathrm{E}_1|^2 + |\mathrm{E}_2|^2 \right). \tag{2.12}$$

where j = 1, 2, and the four terms describe second-harmonic generation (SHG), sum-frequency generation (SFG), difference-frequency generation (DFG), and optical rectification (OR), respectively.

In a more general case, if the input field is polychromatic, i.e., if it has a finite bandwidth as will be discussed later, the second-order nonlinear process can be expressed as [32]

$$P_i(\mathbf{r}, \omega_3) = \varepsilon_0 \sum_{jk} \int_{-\infty}^{\infty} \frac{d\omega_1}{2\pi} \chi_{ijk}^{(2)}(-\omega_3; \omega_1, \omega_2) E_j(\mathbf{r}, \omega_1) E_k(\mathbf{r}, \omega_2). \tag{2.13}$$

Here $\omega_3 = \omega_1 + \omega_2$, and $i = x$, y, or z, so do j and k. Due to the wide bandwidth of the source, any pair of monochromatic components within the source spectrum gives rise to a sum-frequency component through the SFG process, making it possible to realize SFG with a single source.

2.2.2 Nonlinear Optics of Surface Plasmon Polaritons

In 1909, Sommerfield predicted the existence of surface electromagnetic (em) waves [11]. Six decades later, since around 1970, SPPs had become a subject of interest in surface science community as they could be used to probe metal surfaces [12, 19]. At that

time, the success in nonlinear optics had motivated researchers in this area to associate their work with SPPs. It was realized that as the symmetry is broken at an interface, surface nonlinearity of a medium should be different from the bulk nonlinearity. In 1974, Simon et al readily observed SHG by SPPs on a silver film [14], in which the Kretschmann configuration was employed. It has been shown that the resonant coupling of light and collective electron oscillations (plasmons) in noble metals, i.e., SPR, strongly enhances nonlinear optical responses of the medium in the vicinity of air-metal interfaces. After that quite a few works were followed studying this effect under diffrent configurations [35, 36], film compositions [37, 38], thin film thicknesses [39], or surface roughnesses [40]. Meanwhile, besides the fundamental physics, nonlinear excitation of SPPs has been already used in surface sensor applications [41]. The linear process has been extensively employed in the bio-chemical sensor design [3, 13], whereas second- and third-order nonlinear processes are more surface-sensitive, rendering them highly attractive for nonlinear microscopy. In fact, the second-harmonic microscopy has been already proposed and studied [42, 43]. Moreover, since when the new century began, the rise of near-field optics has further advanced the use of nonlinear plasmonics into an even higher level. Nanoscale probes that can convert light into localized energy from the foundation for diffraction-unlimited imaging and intriguing light-mater interactions [44, 45]. These developments include the exciting nonlinear optical nano antennas [46].

Nevertheless, to the best of our knowledge, nonlinear studies of plasmonics have never considered the spectral response – majority of previous works use photon-detection devices, e.g., charged-coupled device (CCD) camera, to record the scattered nonlinear fields. In a recent study of SHG from the Kretschmann configuration [16], such a CCD camera is employed to receive the far-field reflected nonlinear signal. Shown in Fig. 2.4 that it is only capable of capturing photon energy, whereas no spectral information can be found. As SPP generation is associated with the interaction between incident light photons and thin metal film electrons, it may change the population of photons in the output reflected wave, and leave signature in the far-field that can be detected using spectroscopy techniques. This may create a new dimension, i.e., the spectral domain, to the studies and applications of nonlinear plasmonics. Thus, we need to consider a light model that contains spectral information.

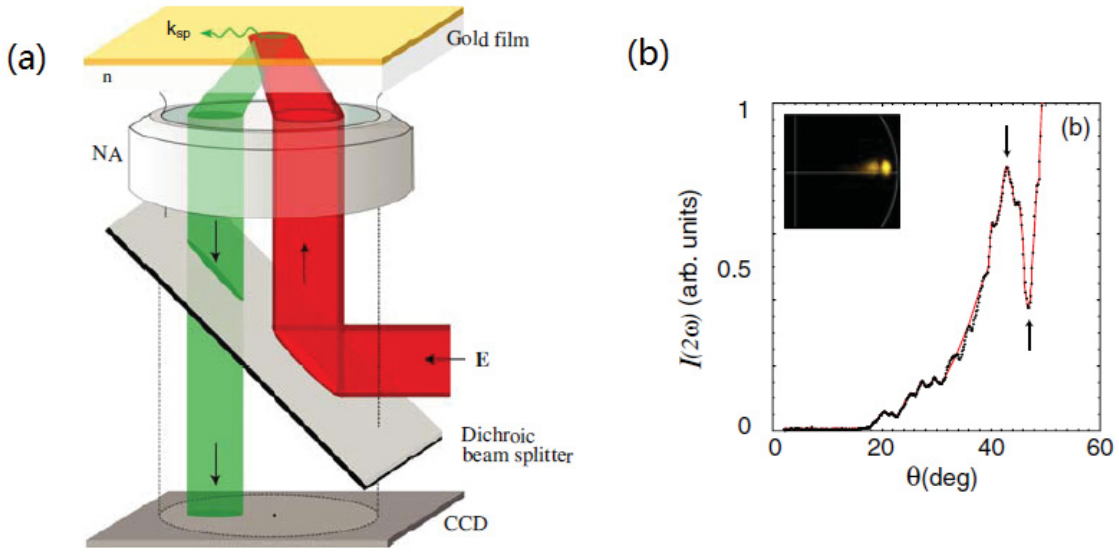

Figure 2.4 (a) The Kretschmann configuration with a CCD camera being the reflected nonlinear field detector. (b) SHG field intensity at a wavelength of λ = 1162 nm as a function of incidence angle. The inset shows an image of the recorded second harmonic light on the CCD camera. No spectral information can be provided (figure sources: Fig. 1 & Fig. 3, [16]).

2.3 Polychromatic Light

Lasers, based on stimulated emission of electromagnetic radiation [30], differ from other sources of light because they generate light coherently. The high temporal coherence allows them to emit a single color of light (*monochromatic*), i.e., have a very narrow spectrum. A necessary background for material to follow in this thesis is the propagation of light wave generated by laser. As the most simplified model, the plane wave is commonly used in basic theoretical studies. In the case shown in Fig. 2.5, this plane wave has the form of

$$\mathbf{E}_m(x,t) = \mathbf{e}_y A_0 e^{i(kx-\omega t)}, \tag{2.14}$$

which represents a linearly polarized, spatially homogeneous, and monochromatic light wave propagating along the *x*-axis.

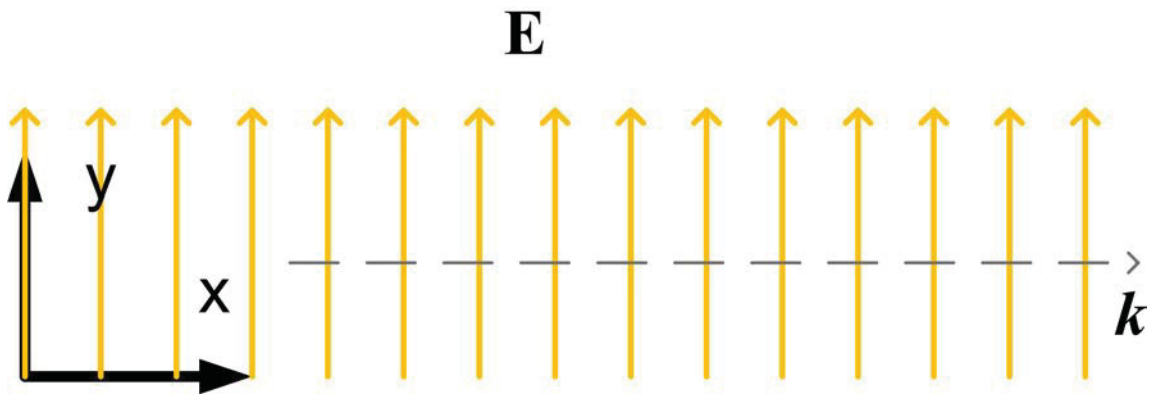

Figure 2.5 Linearly polarized and spatially homogeneous plane wave in free space.

Nevertheless, with the recent development of ultrashort laser pulses and ultrafast optics [47], the pulsed nature of the source will result in a considerable finite bandwidth, such as wideband or even broadband light. This effect has brought about new optical phenomena of interest in plasmonics [17, 18]. Therefore, we need to consider a more realistic, namely, a *polychromatic* plane wave model [48, 49]. To this end, we assume the source has an energy spectrum of $S(\omega)$. Since we are looking for a plane wave result, it has a relation of $S(\omega) \propto |\mathbf{E}|^2 = |A(\omega)|^2$, where $A(\omega)$ is the spectral amplitude. A fully spatially coherent polychromatic light field can then be represented as

$$\mathbf{E}_p(x,\omega) = \mathbf{e}_y A(\omega) e^{i(kx-\omega t)}. \tag{2.15}$$

If Eq. (2.15) is applied to an optical system, e.g., a photonic crystal or the Kretschmann configuration, an output energy spectrum can be obtained. Comparing it with the source energy spectrum allows us to do the spectral analysis. The spectral analysis of radiation, i.e., spectroscopy, is one of the most important analytic methods in science studying the interaction between matter and radiated energy. Historically, spectroscopy originated through the study of visible light dispersed according to its wavelength, e.g., by a prism.

Later the concept was expanded greatly to comprise any interaction with radiative energy as a function of its wavelength or frequency. These interactions include absorption, emission, and so on.

In the next chapter, we are going to study by the presence of SPR, what spectral signatures will be left through the surface nonlinear optical process, to better understand the generation of SPPs and to possibly trigger the future assistant of spectroscopy techniques to nonlinear plasmonics.

CHAPTER 3 Plasmon-Enhanced Spectral Changes in Surface Sum-Frequency Generation with Polychromatic Light

Luyu Wang, Franklin Che, Sergey A. Ponomarenko, and Zhizhang (David) Chen

Published in: Optics Express, June 2013, Vol. 21, 14159

URL: http://www.opticsinfobase.org/oe/abstract.cfm?uri=oe-21-12-14159

3.1 Abstract

We theoretically explore the spectral behavior of the fundamental and sum-frequency waves generated from the surface of a thin metal film in the Kretschmann configuration with coherent ultrashort pulses. We show that the spectra of reflected sum-frequency waves exhibit pronounced shifts for the incident fundamental waves close to the plasmon coupling angle. We also demonstrate that the scale of discovered plasmon-enhanced spectral changes is strongly influenced by the magnitude of the incidence angle and the bandwidth of the source spectrum.

3.2 Introduction

The field of plasmonics has lately experienced a truly explosive growth [50]. Much research in plasmonics has so far been focused on linear light-matter interaction modalities [21, 51], owning largely to the success of plasmonic-based sensors as a powerful tool for probing surfaces [3, 13]. However, resonantly enhanced local electric fields bring about pronounced enhancement of nonlinear responses of plasmonic materials as well [50]. To date, several plasmonenhanced nonlinear optical phenomena have been explored, including second-harmonic generation (SHG) from deterministic [14, 52], random [53–55], and phase-matched [56] nanostructured surfaces. While SHG can be realized with a quasi-monochromatic light source of a fundamental wave (FW),

the sum-frequency generation (SFG) [57, 58] or difference-frequency generation (DFG) [59] in plasmonic materials is more difficult to realize experimentally; this is because it requires two such sources with distinct carrier frequencies as, in general, does surface plasmon excitation by four-wave mixing [15, 16]. These second- and third-order nonlinear processes are surface sensitive at the molecular level, rendering them highly attractive for nonlinear microscopy. In fact, one such modality, the second-harmonic microscopy, has already been proposed and studied [42, 43].

Although the vast majority of work in plasmonics deals with quasi-monochromatic light, there has been growing interest in spectral signatures of plasmon enhanced electromagnetic fields. In particular, the *linear* optical response of homogenous [17] and inhomogeneous–periodic or random [18]–plasmonic nanostructures, probed with broadband light beams, has been recently examined. However, to the best of our knowledge, plasmon-enhanced *nonlinear* optical processes, excited by polychromatic light sources, have not yet been studied. In this context, it is especially instructive to learn whether plasmons, excited on the surface of a conducting material or nanostructure, leave any signatures in the far-field spectra of generated second-order nonlinear waves. The affirmative answer to this question can trigger new developments in surface nonlinear spectroscopy, microscopy, and surface morphology studies.

In this work, we investigate the spectral behavior of the fundamental and sum-frequency waves in the surface SFG from a thin metal film with the polychromatic incident light. We assume that the source field is well collimated such that it can be treated as a plane wave. The wide bandwidth of the source makes it possible to realize SFG with a single source: any pair of monochromatic components within the source spectrum gives rise to a sum-frequency component through the surface SFG process. For symmetric source spectra, one would expect the SFG spectrum to peak at half the carrier wavelength of the source. We show, however, that at the incidence angle corresponding to light coupling to the surface plasmon, the reflected sum-frequency wave (SFW) spectrum gets blue-shifted from the expected maximum whereas the reflected FW has a spectral hole at the carrier frequency. We further demonstrate that the magnitude of the effect depends on the bandwidth of the source spectrum and the incidence angle: the shifts of SFW spectra become more pronounced as the source bandwidth increases, while

at a certain angle a spectral switch is observed. Also, as the incidence angle deviates from the plasmon coupling angle, all spectral changes disappear. The appearance of large SFW shifts can serve as an unambiguous plasmon signature in nonlinear surface spectroscopy.

3.3 THEORY

We consider fully spatially coherent incident light [48, 49], which we assume to behave as a plane wave. We examine the spectral behavior of fundamental and sum-frequency waves in the Kretschmann geometry [12] illustrated in Fig. 1. A thin metal (gold) film is illuminated by a *p*-polarized polychromatic plane wave from glass ($\varepsilon_1 = 2.25$) at the angle of incidence θ_i. The gold film has a thickness d and relative dielectric permittivity $\varepsilon_2(\omega)$. The incident wave with the spectral amplitude $A(\omega)$ can be represented as

$$\mathbf{E_i}(x,z,\omega,\theta_i) = A(\omega)\left(\frac{k_{1z}}{k_1}\mathbf{e_x} - \frac{k_x}{k_1}\mathbf{e_z}\right)e^{i(k_x x + k_{1z} z)}, \tag{3.1}$$

where $\mathbf{k}_1 = (k_x,\ 0,\ k_{1z})$ and $k_1 = \omega\sqrt{\mu_0\varepsilon_1}$; $\mathbf{e}_x$ and $\mathbf{e}_z$ are unit vectors in the *x*- and *z*-directions, respectively. The components of the wave vector $\mathbf{k}_1$ can be expressed as $k_x = k_1\sin\theta_i$ and $k_{1z} = k_1\cos\theta_i$. The finite bandwidth of the incident light can originate either from partial temporal coherence or from a pulsed nature of the source. We assume henceforth that the incident light wave is produced by a coherent femtosecond laser source which provides sufficiently large input intensities to generate a nonlinear optical response of the system. Thus, we introduce the energy spectrum of the incident pulse by the expression [60]

$$S_i(\omega) \propto \left|\mathbf{E}_i(x,z,\omega,\theta_i)\right|^2 = \left|A(\omega)\right|^2, \tag{3.2}$$

up to an immaterial proportionality constant.

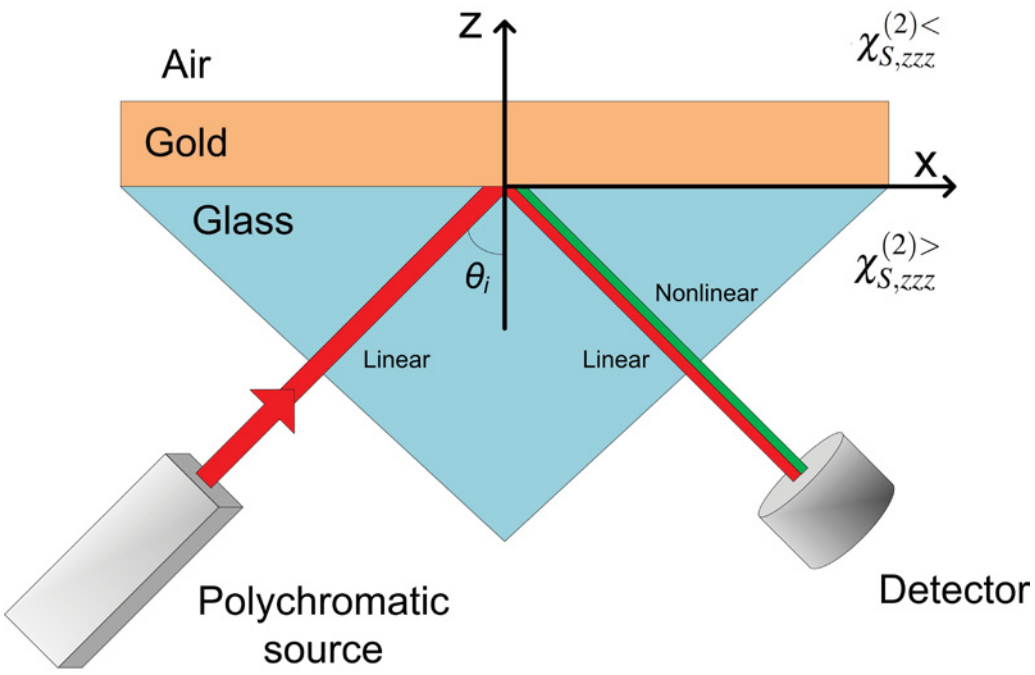

Figure 3.2 Illustrating the Kretschmann configuration.

The (multiply) reflected FW strikes the detector. Using the standard multiple-reflection Airy method (for details see Appendix A), it can be inferred that the reflected wave is

$$E_r(x,z,\omega,\theta_i) = A(\omega)(-\frac{k_{1z}}{k_1}\mathbf{e_x} - \frac{k_x}{k_1}\mathbf{e_z})\tilde{r}_{12}(\omega,\theta_i)e^{i(k_x x - k_{1z} z)}. \tag{3.3}$$

The reflected energy spectrum can then be written as

$$S^{(1)}(\omega,\theta_i) \propto \left|\mathbf{E}_r(x,z,\omega,\theta_i)\right|^2 \propto \left|\tilde{r}_{12}(\omega,\theta_i)\right|^2 S_i(\omega). \tag{3.4}$$

Here $\tilde{r}_{12}(\omega,\theta_i)$ is the double-interface Fresnel reflection coefficient for *p*-polarization given by [61]

$$\tilde{r}_{12}(\omega,\theta_i)=\frac{r_{12}+r_{23}e^{i2k_{2z}d}}{1+r_{12}r_{23}e^{i2k_{2z}d}}, \tag{3.5}$$

where $k_{2z}=\sqrt{k_2^2-k_x^2}$.

Next, the FW gives rise to nonlinear polarizations on both interfaces of the film. In general, the *i*'th component (*i* = *x, y*, or *z*) of the sum-frequency polarization field can be written as [32]

$$P_i(\mathbf{r},\omega_3)=\varepsilon_0\sum_{jk}\int_{-\infty}^{\infty}\frac{d\omega_1}{2\pi}\chi^{(2)}_{ijk}(-\omega_3;\omega_1,\omega_2)E_j(\mathbf{r},\omega_1)E_k(\mathbf{r},\omega_2), \tag{3.6}$$

where ω_1 and ω_2 are pump frequencies while $\omega_3 = \omega_1 + \omega_2$ represents the generated nonlinear frequency, and $\mathbf{r}$ = (*x*, *y*, *z*); $\chi^{(2)}_{ijk}(-\omega_3;\omega_1,\omega_2)$ is the nonlinear susceptibility tensor of the sum-frequency generation (SFG) process. The subscripts denote the Cartesian field components tangential and normal to the interface, respectively. It was argued theoretically [62] that at relatively large pump wavelengths ($\lambda \geq 690$ nm for gold), the leading contribution to the nonlinear polarization comes from the diagonal surface component $\chi^{(2)}_{S,zzz}$ of the second-order susceptibility tensor. This claim is supported with the available SHG experimental data [63, 64], and it has been recently employed in a surface DFG study [59]. Hence, we will ignore the other contributions to $\chi^{(2)}$ hereafter. Therefore, we will only need the *z*-component of the field at the top and bottom of the film to determine the polarization fields in Eq. (3.6).

It can be shown that the total FW field in the glass is simply a superposition of the incident and reflected waves in Eqs. (3.1) and (3.3), respectively. The normal component of the reflected electric field is then

$$E_{1z}(x,z,\omega,\theta_i)=-\frac{k_x}{k_1}A(\omega)e^{ik_x x}\left[e^{ik_x x}+\tilde{r}_{12}(\omega,\theta_i)e^{-ik_{1z}z}\right]. \tag{3.7}$$

The field on the lower interface can be found by taking z = 0. In addition, on applying the boundary condition for the normal components of the field on both sides of the lower interface, we obtain the field on the metal side of the lower interface as

$$E_{2z}^{<}(x,\omega,\theta_i) = -\frac{k_x}{k_1}\frac{\varepsilon_1}{\varepsilon_2}A(\omega)e^{ik_x x}\left[1+\tilde{r}_{12}(\omega,\theta_i)\right]. \tag{3.8}$$

Similarly, the total FW field in the film is a superposition of the waves transmitted and reflected by the upper interface. The corresponding normal component of the field can be represented as

$$E_{2z}(x,z,\omega,\theta_i) = -\frac{k_x}{k_2}A(\omega)e^{ik_x x}\frac{t_{12}}{1+r_{12}r_{23}e^{i2k_{2z}d}}\left[e^{ik_{2z}z}+r_{23}e^{i2k_{2z}d}e^{-ik_{2z}z}\right]. \tag{3.9}$$

At the upper interface $z = d$, we have

$$E_{2z}^{>}(x,\omega,\theta_i) = -\frac{k_x}{k_2}A(\omega)e^{ik_x x}R(\omega,\theta_i), \tag{3.10}$$

where

$$R(\omega,\theta_i) = \frac{t_{12}(1+r_{23})e^{ik_{2z}d}}{1+r_{12}r_{23}e^{i2k_{2z}d}}. \tag{3.11}$$

On substituting from Eqs. (3.8) and (3.10) into Eq. (3.6), the polarization fields at the upper and lower interfaces read

$$\mathbf{P}^{<}(x,\omega_3,\theta_i) = \mathbf{e_z}P_0^{<}(\omega_3,\theta_i)e^{ik_x(\omega_3)x}, \tag{3.12}$$

$$\mathbf{P}^{>}(x,\omega_3,\theta_i) = \mathbf{e_z}P_0^{>}(\omega_3,\theta_i)e^{ik_x(\omega_3)x}, \tag{3.13}$$

where $k_x(\omega_3) = k_1(\omega_3)\sin\theta_i$, $k_1(\omega_3) = \omega_3\sqrt{\mu_0\varepsilon_1}$, and we introduced

$$P_0^{<}(\omega_3,\theta_i) = \varepsilon_0\varepsilon_1^2\sin^2\theta_i\int_{-\infty}^{\infty}\frac{d\omega_1}{2\pi}\chi_{S,zzz}^{(2)<}(-\omega_3;\omega_1,\omega_2)$$
$$\times\frac{A(\omega_1)A(\omega_2)}{\varepsilon_2(\omega_1)\varepsilon_2(\omega_2)}\left[1+\tilde{r}_{12}(\omega_1,\theta_i)\right]\left[1+\tilde{r}_{12}(\omega_2,\theta_i)\right], \tag{3.14}$$

and

$$P_0^{>}(\omega_3,\theta_i) = \varepsilon_0\varepsilon_1\sin^2\theta_i\int_{-\infty}^{\infty}\frac{d\omega_1}{2\pi}\chi_{S,zzz}^{(2)<}(-\omega_3;\omega_1,\omega_2)$$
$$\times\frac{A(\omega_1)A(\omega_2)}{\sqrt{\varepsilon_2(\omega_1)\varepsilon_2(\omega_2)}}R(\omega_1,\theta_i)R(\omega_2,\theta_i), \tag{3.15}$$

These polarizations act as the sources of secondary upconverted SFW. The *i*'th Cartesian component of the resulting sum-frequency field is determined from Maxwell's equations to be

$$E_i(r,\omega) = \frac{(\omega/c)^2}{\varepsilon_0}\sum_j\int d\mathbf{r}'G_{ij}(\mathbf{r},\mathbf{r}',\omega)P_j(\mathbf{r}',\omega). \tag{3.16}$$

Here $G_{ij}(\mathbf{r},\mathbf{r}',\omega)$ is the dyadic Green's tensor which can be expressed as [21]

$$G_{ij}(\mathbf{r},\mathbf{r}',\omega) = \left[\delta_{ij} + \frac{1}{k^2}\nabla_i\nabla_j\right]G_0(\mathbf{r},\mathbf{r}',\omega), \tag{3.17}$$

where $G_0(\mathbf{r},\mathbf{r}',\omega)$ is the scalar free-space Green's function representing an outgoing spherical wave from a point source. We use the Weyl identity to expand the spherical wave into an angular spectrum of plane waves [21, 48]

$$G_0(\mathbf{r},\mathbf{r}',\omega)=\frac{e^{ik|\mathbf{r}-\mathbf{r}'|}}{4\pi|\mathbf{r}-\mathbf{r}'|}=\frac{i}{8\pi^2}\int_{-\infty}^{\infty}\frac{dk_x}{k_z}e^{ik_x(x-x')+ik_z(z-z')}. \tag{3.18}$$

Note that the problem we study is two-dimensional implying that **r** = (*x*, 0, *z*) and **r'** = (*x'*, 0, *z'*). The nonlinear polarization field at the lower interface $P^{<}$ gives rise to a contribution to the SFW through the field directly reflected into the lower half-space. It can be obtained by substituting from Eqs. (3.12) and (3.17) into Eq. (3.16), and using Eq. (3.18), yielding

$$\mathbf{E}^{(2)<}_{down}(x,z,\omega_3,\theta_i)=\frac{i\omega_3\sin\theta_i}{8\pi^2\varepsilon_0 c\sqrt{\varepsilon_1}}P_0^{<}(\omega_3,\theta_i)(-\mathbf{e_x}+\tan\theta_i\mathbf{e_z})e^{i[k_x(\omega_3)x-k_{1z}(\omega_3)z]}, \tag{3.19}$$

where $\mathbf{k}_1(\omega_3)=k_x(\omega_3)\mathbf{e_x}+k_{1z}(\omega_3)\mathbf{e_z}$. By the same token, the other contribution from $\mathbf{P}^{<}$ to the SF field, partially transmitted into the film and eventually reflected back to the lower half-space, is

$$\mathbf{E}^{(2)<}_{up}(x,z,\omega_3,\theta_i)=\frac{i\omega_3\sin\theta_i}{8\pi^2\varepsilon_0 c\sqrt{\varepsilon_2(\omega_3)}}P_0^{<}(\omega_3,\theta_i)(-\mathbf{e_x}+\tan\theta_i\mathbf{e_z})$$
$$\times\frac{r_{23}t_{21}e^{i2k_{2z}(\omega_3)d}}{1+r_{12}r_{23}e^{i2k_{2z}(\omega_3)d}}e^{i[k_x(\omega_3)x-k_{1z}(\omega_3)z]}. \tag{3.20}$$

The Fresnel coefficients here are all evaluated at the frequency $\omega_3=\omega_1+\omega_2$ while $k_2(\omega_3)=\sqrt{k_x^2(\omega_3)+k_{2z}^2(\omega_3)}$.

The contribution to the reflected SFW from the nonlinear polarization field at the upper interface $\mathbf{P}^{>}$ is determined as

$$\mathbf{E}^{(2)>}(x,z,\omega_3,\theta_i)=\frac{i\omega_3\sin\theta_i}{8\pi^2\varepsilon_0 c\sqrt{\varepsilon_2(\omega_3)}}P_0^{>}(\omega_3,\theta_i)(-\mathbf{e_x}+\tan\theta_i\mathbf{e_z})$$
$$\times\frac{t_{21}e^{i2k_{2z}(\omega_3)d}}{1+r_{12}r_{23}e^{i2k_{2z}(\omega_3)d}}e^{i[k_x(\omega_3)x-k_{1z}(\omega_3)z]}. \tag{3.21}$$

Finally, combining Eqs. (3.19)—(3.21), the energy spectrum of the reflected SFW in the lower half-space is found to be

$$S^{(2)}(\omega_3,\theta_i) \propto \left|\mathbf{E}^{(2)<}_{down}(x,z,\omega_3,\theta_i)+\mathbf{E}^{(2)<}_{up}(x,z,\omega_3,\theta_i)+\mathbf{E}^{(2)>}(x,z,\omega_3,\theta_i)\right|^2. \qquad (3.22)$$

3.4 RESULTS

We utilize Eqs. (3.4) and (3.22) to evaluate the spectra of FW and SFW at the detector. The laser source is assumed to be tunable, generating ulstrashort pulses of duration ranging from 30 to 90 fs (FWHM). This translates to the bandwidth of approximately 3.33×10^{13} to 1.0×10^{14} s^{-1} assuming a Gaussian pulse profile; typical Ti-sapphire lasers generate femtosecond pulses in this temporal range [47]. The carrier wave length of the source spectrum is assumed to be λ_0 = 1162 nm. The gold film has a thickness of d = 50 nm. To describe linear dielectric properties of the film, we employ a modified Drude-Sommerfeld model which takes into account the contributions from free and bound (interband transitions) electrons resulting in [21]

$$\varepsilon_2(\omega)=1-\frac{\omega_p^2}{\omega^2+i\Gamma\omega}+\frac{\tilde{\omega}_p^2}{\omega_0^2-\omega^2-i\gamma\omega}. \qquad (3.23)$$

The parameters of the model are: plasma frequencies, ω_p = 13.8×10^{15} s^{-1} and $\tilde{\omega}_p$ = 4.5×10^{15} s^{-1}; damping rates, Γ = 1.075×10^{15} s^{-1} and γ = 9×10^{14} s^{-1}; bound electron resonant frequency, ω_0 = 4.187×10^{15} s^{-1}. The surface nonlinear susceptibility is described within the framework of a hydrodynamic model developed in [65]. The leading contribution reads

$$\chi^{(2)}_{S,zzz}(-\omega_3;\omega_1,\omega_2)=-\frac{a(\omega_1,\omega_2)\left[\varepsilon_2(\omega_1)-1\right]\left[\varepsilon_2(\omega_2)-1\right]}{32\pi^2 n_B e}, \qquad (3.24)$$

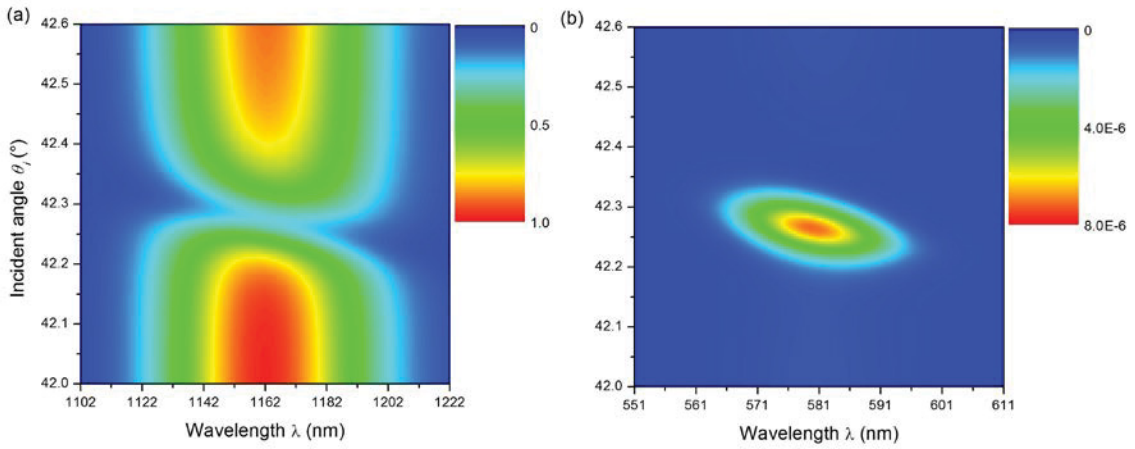

Figure 3.2 Far-field energy spectra of (a) FW and (b) SFW around the plasmon coupling angle. The source pulse durations is $t_p = 90$ fs.

where n_B is the equilibrium free-electron density in the bulk. The dimensionless parameter $a(\omega_1, \omega_2)$ is essentially frequency-indipendent whenever the two pump frequencies ω_1 and ω_2 lie well below the volume plasma frequency ωp. In our case, $\Delta\omega < 0.1\omega_0$ and $\omega_0/\omega_p \approx 0.117$, implying that any frequency within the source bandwidth is much smaller than ω_p. Hence, we may safely treat $a(\omega_1, \omega_2)$ as a constant. The evaluated $\chi^{(2)}_{S,zzz}(-\omega_3; \omega_1, \omega_2)$ is then of the order of 10^{-18} m^2/V (10^{-12} cm^2/statvolt in Gaussian units), showing excellent agreement with the experimental results of [64].

The plasmon coupling angle is given by [21]

$$\theta_c(\omega) = \sin^{-1}\sqrt{\frac{\varepsilon_2(\omega)}{\varepsilon_1\left[\varepsilon_2(\omega)+1\right]}}\,. \tag{3.25}$$

In our case, $\theta_c(\omega_0) \approx 42.3°$. Under these conditions, free electrons in the film respond collectively to incident light waves by oscillating in resonance with the FW, i.e., surface plasmon resonance (SPR) occurs. It can be clearly seen in Fig. 3.2(a) that due to the efficient coupling to surface plasmons, the reflected FW has a hole in the far-field spectrum. The electromagnetic energy is localized near the film-air interface, dramatically enhancing the efficiency of SFG. The generated SFW is then reflected from

the glass back to the detector and a large spectral peak, clearly visible in Fig. 2(b), is registered. Notice that the SFW is much better localized than the FW. For symmetric source spectra, one would expect the SFW spectrum to have a maximum at half the carrier wavelength of the FW (581 nm). However, the peak is actrally blue-shifted with respect to the expected position. We conclude that the SPR leaves unambiguous signatures in the far-field spectrum of generated SFW.

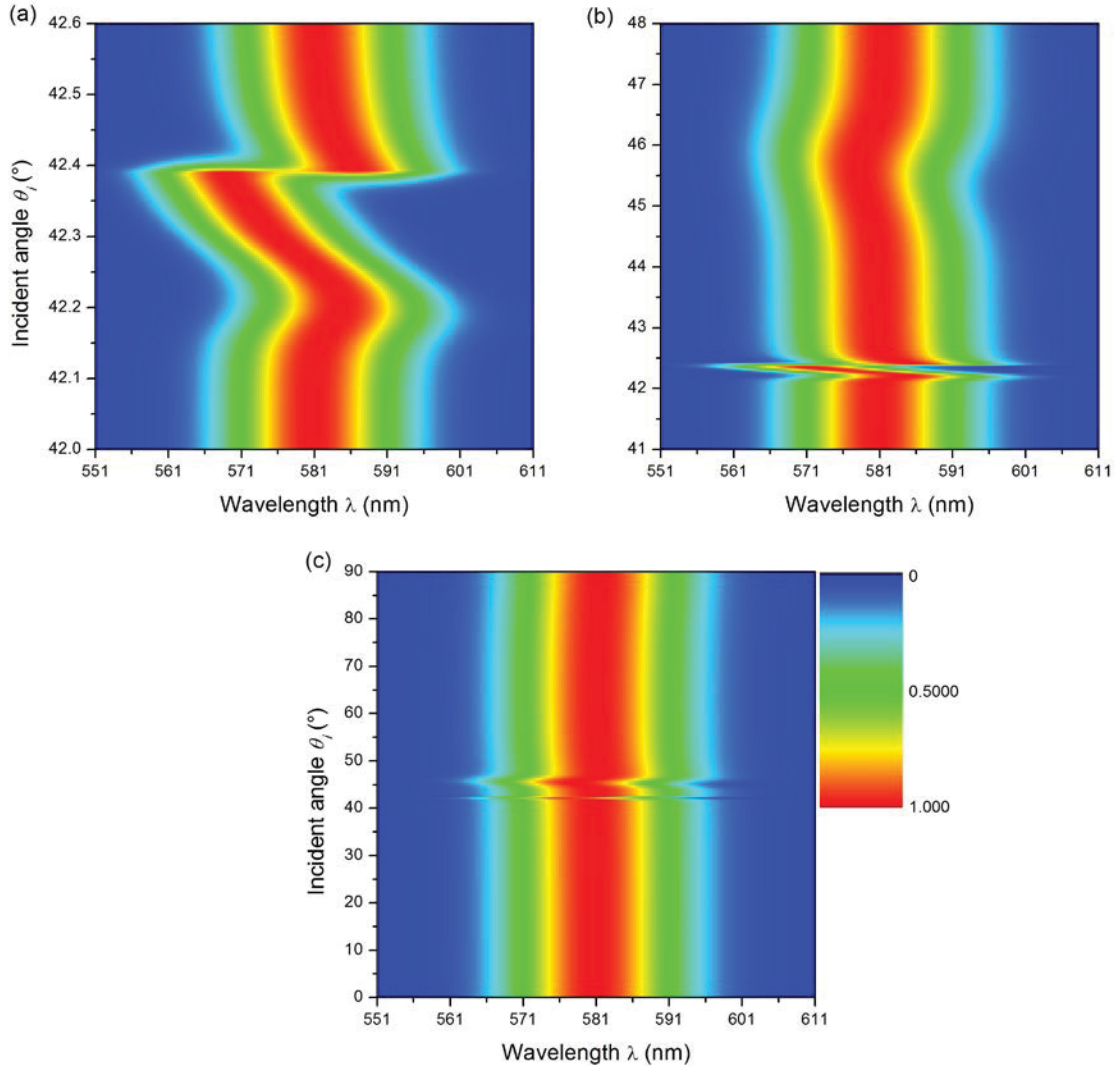

Figure 3.3 Normalized far-field SFW energy spectrum for different incident angle ranges. The source pulse duration is $t_p = 90$ fs.

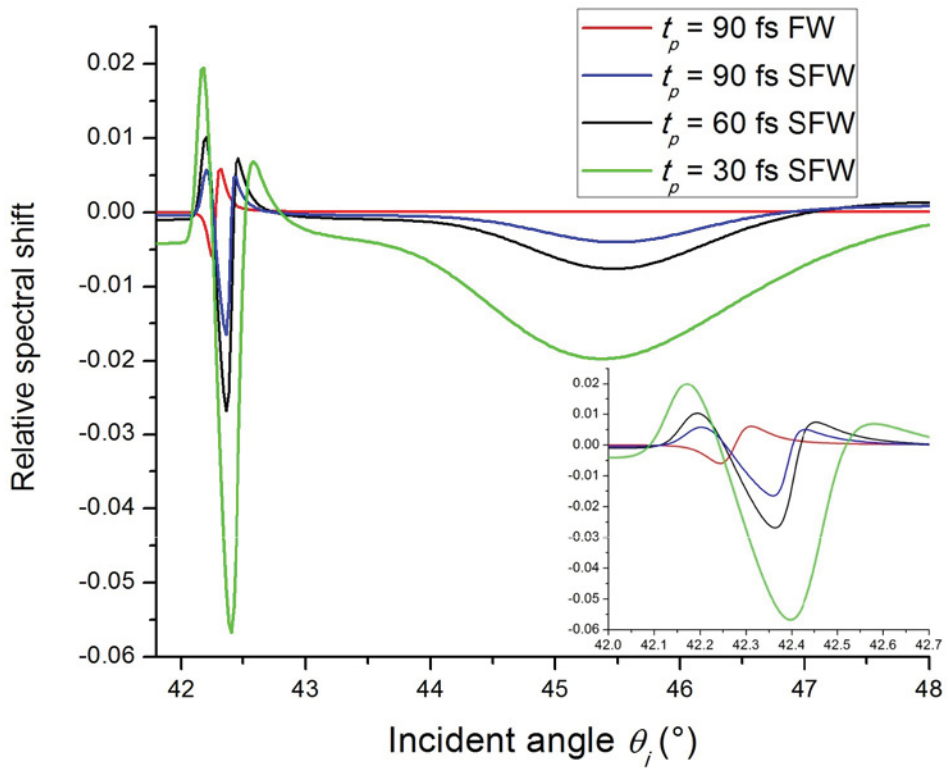

Figure 3.4 Relative shifts of mean fundamental (sum-frequency) wavelengths at different incident angles with respect to the (half) pump carrier wavelength for different source pulse durations. Insert shows relative spectral shifts for incidence angles in the vincinity of the plasmon coupling angle. Negative values indicate blue shifts.

To better illustrate spectral aspects of SFG in the system, we normalize the SFW spectrum of Fig. 3.2(b) to the corresponding maximum value for each θ_i and display the result in Fig. 3.3. In Fig. 3.3(a), we exhibited the SFW spectrum in a narrow range of incidence angles around the plasmon coupling angle. It can be inferred from the figure that the SPR gives rises to an overall blue-shift of the SFW spectrum. Displaying a wider incidence angle range in Fig. 3.3(b), we can observe that there is another (smaller) spectral shift toward the blue around 46°. This results from the SPR at SFW wavelengths: as long as the SFW is generated due to the strong FW enhancement, it can also be coupled to surface plasmons resulting in SPR excitation in the SFW. The corresponding plasmon coupling angle can be determined from the equation identical to Eq. (3.25), except ε_2 is evaluated at $2\omega_0$ leading to $\theta_c^{(2)}(2\omega_0) \approx 45.6°$. As is seen in Fig. 3.3(c),

which shows the SFW spectrum on an even larger scale, the spectrum is consistently centered at 581 nm for incidence angles ranging from 0 to 90°, except in the neighborhood of linear and nonlinear SPRs. As the incidence angle deviates a little from θ_c or $\theta_c^{(2)}$, the magnitude of the corresponding spectral shift falls off precipitously.

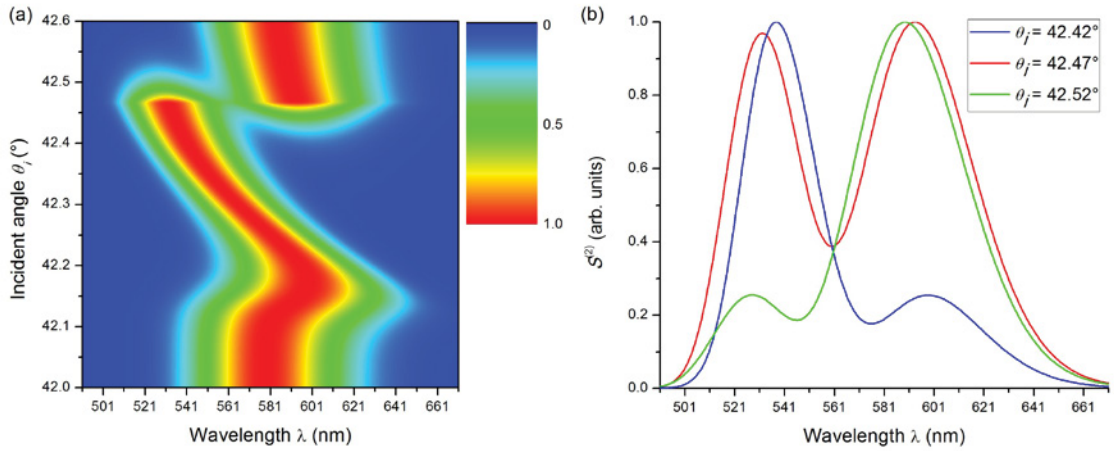

Figure 3.5 (a) Normalized far-field SFW energy spectrum in the vicinity of the plasmon coupling an.gle with an incident pulse duration of t_p = 30 fs. (b) The SFW spectral switch

We can also show that the magnitude of discovered spectral changes is strongly influenced by the bandwidth of the source spectrum. To drive this point home, we display in Fig. 3.4 relative shifts of the mean fundamental (sum-frequency) wavelength relative to the (half) pump carrier wavelength as functions of the incidence angle for different pulse durations. It can be inferred from the figure that the shorter the pulse duration, the larger the spectral shift. More specifically, as we increase the source bandwidth, a sharp transition from blue to red in the vicinity of the plasmon coupling angle, seen in Fig. 3.3(a), transforms to a spectral dip. We observe such a spectral switch in Fig. 3.5(a) at θ_i = 42.47° for the input pulse of t_p = 30 fs duration. Qualitatively, the present spectral switch is similar to the one previously discovered in Fraunhofer diffraction of light by a circular aperture [66]. We note that for the incidence angles outside the immediate neighborhood of the switch angle, the SFW spectrum displays no anomalous features,

remaining Gaussian-like. We stress that the appearance of extremely surface-sensitive features in the reflected SFW spectrum can provide for environmental sensing with unprecedented accuracy. Indeed, any tiny perturbation of the film surface, leading to the corresponding change in the refractive index, can cause a switch of the SFW spectrum. Although the principle has been previously employed in conventional linear plasmonic sensor configurations [3, 13, 21], the use of *nonlinear* wave spectra can help attain, perhaps, a single-atom level of accuracy. This point is illustrated in Fig. 3.5(b) where we show that the SFW spectral behavior at the switch angle is sensitive to the angle variations of just a fraction of a degree.

3.5 Summary

To summarize, we theoretically explored the spectral behavior of surface-enhanced sum-frequency generation from a thin metal film produced with coherent ultrashort laser pulses. We have shown that while spectra of fundamental waves, reflected at the angle corresponding to surface plasmon excitation in the film, can have a hole at the carrier freqency, the resonantly enhanced sum-frequency waves display pronounced spectral shifts. Thus, excited surface plasmons leave characteristic signatures in the spectra of fundamental and sum-frequency waves. We have also revealed that the discovered spectral changes strongly depend on the incidence angle and the bandwidth of the source spectrum, as well as observed a spectral switch which is sensitive to the angle variations. Our results may open up new avenues in nonlinear spectroscopy, surface plasmon sensing, and surface morphology studies.

CHAPTER 4 CONCLUSION REMARKS AND RECOMMENDATIONS

4.1 Conclusion Remarks

In this thesis, we have presented the first exploration of the spectral behavior of nonlinear plasmonics. We theoretically studied surface-enhanced sum-frequency generation from a thin gold film utilized with coherent ultrashort laser pulses.

The Kretschmann configuration, the platform of this work, is modeled as a planarly layered media, allowing us to describe the wave propagations in the film. The nonlinear polarizations are then found which can act as secondary sources of reflected SFW. We utilize the Lorentz-Drude model to characterize the dielectric permittivity of the gold film, and a hydrodynamic model to represent the weakly dispersive nonlinear susceptibility. At last, we employ Green's function method to express the final far-field SFW spectrum.

We have shown that when the incidence angle approaches the angle corresponding to surface plasmon excitation in the film, the spectra of fundamental waves can have a hole at the carrier freqency, whereas the resonantly enhanced sum-frequency waves exhibit spectacular spectral shifts. Thus, excited surface plasmons leave characteristic yet totally different signatures in the far-field spectra of fundamental and sum-frequency waves.

We have also revealed that the discovered spectral shifts shrongly depend on the incidence angle. When it is away from the plasmon coupling angle, the spectrum stays steady at the anticipated nonlinear frequency – only when the angle is in the close neighbourhood of SPR generation, the spectrum will shift to an unusual frequency. This is useful to easily and accurately detect SPR using spectroscopy techniques.

Another finding is that when tuning the duration of input laser pulse, the shifts will be strongly affected: the shorter the input pulse is, the more the spectrum shifts. This may make it possible to engineer the output spectra with tunable lasers readily available.

Last but not least, we have observed a spectral switch which is extremely sensitive to the angle variations. Although previously linear plasmonic surface sensors have been

taking advantage of this kind of feature, the appearance of it in the nonlinear spectrum holds promise for surface environmental sensing with unprecedented accuracy.

In summary, our results may trigger new developments in surface nonlinear spectroscopy, microscopy, surface plasmon sensing, and surface morphology studies.

4.2 Recommendations for Future Work

There are several topics of future research that can be pursued further.

First of all, this work definitely requires future experiment verification of the discovered spectral changes.

Next, we made use of a plane wave model to describe the input laser field. To be more accurate, using a beam model with characteristic spatial field distribution, e.g., angular spectrum representation of a Gaussian beam, or even high order Hermite-Gaussian beams, may reveal even more valuable information.

Also, except for SFG we have studied in this thesis, other nonlinear processes such as DFG or some third-order nonlinear processes could also leave unique spectral signature.

Finally, we found that the film thickness can affect the shifts dramatically. However, the mechanism under this effect has not been fully understood yet.

BIBLIOGRAPHY

[1] S. A. Maier, Plasmonics: Fundamentals and Applications (Springer Science, 2007).
[2] E. Ozbay, "Plasmonics: Merging Photonics and Electronics at Nanoscale Dimensions," Science 189, 189–193 (2006).
[3] J. Homola, S. S. Yee, and G. Gauglitz, "Surface plasmon resonance sersors: review," Sensors and Actuators B 54, 3–15 (1999).
[4] H. A. Atwater, "The Promise of Plasmonics," Scientific American 296, 56–63 (2007).
[5] J.-S. Bouillard, S. Vilain, W. Dickson, and A. V. Zayats, "Hyperspectral imaging with scaning near-field optical microscopy: applications in plasmonics," Opt. Express 18, 16513 (2010).
[6] K. Y. Yang, K. C. Choi, and C. W. Ahn, "Surface plasmon-enhanced spontaneous emission rate in an organic light-emitting device structure: cathode structure for plasmonic application," Appl. Phys. Lett. 94, 173301 (2009).
[7] M. I. Stockman, "Nanoplasmonics: The physics behind the applications," Phys. Today 64, 39–44 (2011).
[8] W.-K. Fong, T. L. Hanley, B. Thierry, N. Kirby, and B. J. Boyd, "Plasmonic Nanorods Provide Reversible Control over Nanostructure of Self-Assembled Drug Delivery Materials," Langmuir 26, 6136-6139 (2010).
[9] M. Ozaki, J. Kato, and S. Kawata, "Surface-plasmon holography with white-light illumination," Science 332, 218–220 (2011).
[10] H. A. Atwater and A. Polman, "Plasmonics for improved photovoltaic devices," Nat. Mater. 9, 205–213 (2010).
[11] A. Sommerfeld, "Über die Ausbreitung der Wellen in der drahtlosen Telegraphie," Ann. d. Phys., 28, 665-36 (1909).
[12] E. Kretschmann and H. Raether, "Radiative decay of non-radiative surface plasmons excited by light," Z. Naturforsch. A 23, 2135-2136 (1968).
[13] L. M. Zhang and D. Uttamchandani, "Optical chemical sensing employing surface plasmon resonance," Electron. Lett. 23, 1469–1470 (1988).
[14] H. J. Simon, D. E. Mitchell, and J. G. Watson, "Optical second-harmonic generation with surfance plasmons in silver films," Phys. Rev. Lett. 33, 1531–1534 (1974).
[15] F. DeMartini, F. G. Giuliani, M. Mataloni, E. Palange, and Y. R. Shen, "Study of Surface Polaritons in GaP by Optical Four-Wave Mixing," Phys. Rev. Lett. 37, 440-443 (1976).
[16] S. Palomba and L. Novotny, "Nonlinear Excitation of Surface Plasmon Polaritons by Four-Wave mixing," Phys. Rev. Lett. 101**,** 056802 (2008).
[17] T.-H. Lan, Y.-K. Chyng, J. Li, and C.-H. Tien, "Plasmonic rainbow rings induced by white radial polarization," Opt. Lett. 37, 1205–1207 (2012).
[18] Y. Nishijima, L. Roza, and S. Juodkazis, "Surface plasmon resonances in periodic and random patterns of gold nano-disks for broadband light harvesting," Opt. Express 20, 11466 (2012).
[19] A. Otto, "Excitation of nonradiative surface plasma waves in silver by the method of frustrated total reflection," Z. Phys. 216, 398-410 (1968).

[20] P. Bharadwaj, A. Bouhelier, and L. Novotny, "Electrical Excitation of Surface Plasmons," Phys. Rev. Lett. 106, 226802 (2011).
[21] L. Novotny and B. Hechi, *Principles of Nano-Optics* (Cambridge University, 2006).
[22] R. P. Duyne, "Molecular Plasmonics," Science 306, 985–986 (2004).
[23] F. Lopez-Tejeira, S. G. Rodrigo, L. Martin-Moreno, F. J. Garcia-Vidal, E. Devaux, T. W. Ebbesen, J. R. Krenn, I. P. Radko, S. I. Bozhevolnyi, M. U. Gonzalez, J. C. Weeber, and A. Dereux, "Efficient unidirectional nanoslit couplers for surface plasmons," Nature Physics 3, 324–328 (2007).
[24] M. Rajarajan, C. Themistos, B. M. A. Rahman, and K. T. V. Grattan, "Plasmonics in Metal-clad Terahertz Waveguides," Prog. Electromagn. Res. 3, 294–299 (2007).
[25] W. L. Barnes, A. Dereux, and T. W. Ebbesen, "Surface plasmon subwavelength optics," Nature 424, 824–830 (2003).
[26] S. A. Maier, "Plasmonics – Towards Subwavelength Optical Devices," Current Nanoscience 1, 17–22 (2005).
[27] R. Zia, J. A. Schuller, A. Chandran, and M. L. Brongersma, "Plasmonics: the next chip-scale technology," Materials Today 9, 20–27 (2006).
[28] M. L. Brongersma, R. Zia, and J. Schuler, "Plasmonics – The Missing Link between Nanoelectronics and Microphotonics," Appl. Phys. A 89, 221-223 (2007).
[29] M. Born and E. Wolf, *Principles of Optics* (Pergamon, 1989).
[30] T. H. Maiman, "Stimulated optical radiation in ruby," Nature 187(4736), 493–494 (1960).
[31] P. A. Franken, A. E. Hill, C. W. Peters, and G. Weinreich, " Generation of optical harmonics," Phys. Rev. Lett. 7, 118-120 (1961).
[32] R. W. Boyd, *Nonlinear Optics*, II ed. (Academic, Boston, 2003).
[33] Y. R. Shen, "Surface Nonlinear Optics: A Historical Perspective," IEEE J. Sel. Top. Quantum Electron. 6, 1375-1379 (2000).
[34] M. Kauranen and A. V. Zayats, "Nonlinear plasmonics," Nat. Photonics 6, 737-748 (2012).
[35] J. G. Rako, J. C. Quail, and H. J. Simon, "Optical second-harmonic generation with surface plasmons in noncentrosymmetric crystals." Phys. Rev. B 30, 5552-5559 (1984).
[36] C.-C. Tzeng and J. T. Lue, "Nonlinear optical generation from noble metals and aluminum films in various geometric configurations," Phys. Rev. A 39, 191-196 (1989).
[37] J. C. Quail and H. J. Simon, "Second-harmonic generation from silver and aluminum films in total internal reflection," Phys. Rev. B 31, 4900-4905 (1985).
[38] K. Y. Lo and J. T. Lue, "The Detection of Optical Second Harmonic Generation from High Tc $YBa_2Cu_3O_7$ Epitaxial Thin Films," IEEE Photon. Technol. Lett. 6, 1362-1364 (1994).
[39] J.-T. Lue and C.-S. Chang, "Surface Plasmon enhanced optical second harmonic generation in ultra-thin metallic films," J. Nonlinear Opt. Phys. & Mater. 8, 503-518 (1999).
[40] S. I. Bozhevolnyi, K. Pedersen, "Second harmonic generation due to surface plasmon localization," Surf. Sci. 377-379, 384-387 (1997).
[41] R. Naraoka, H. Okawa, K. Hashimoto, and K. Kajikawa, "Surface plasmon resonance enhanced second-harmonic generation in Kretschmann configuration," Opt. Comm. 248, 249-256 (2005).

[42] R. M. Corn and D. A. Higgins, "Optical second harmonic generation as a probe of surface chemistry," Chem. Rev. 94, 107–125 (1994).
[43] J. Vydra and M. Eich, "Mapping of the lateral polar orientational distribution in second-order nonlinear thin films by scanning second-harmonic microscopy," Appl. Phys. Lett. 72, 275–277 (1998).
[44] L. Novotny, "From near-field optics to optical antennas," Phys. Today 64, 47-52 (2011).
[45] P. Bharadwaj, B. Deutsch, and L. Novotny, "Optical Antennas," Adv. Opt. Photon. 1, 438-483 (2009).
[46] H. Harutyunyan, G. Volpe, R. Quidant, and L. Novotny, "Enhancing the nonlinear optical response using multifrequency gold-nanowire antennas," Phys. Rev. Lett. 108, 217403 (2012).
[47] J.-C. Diels and W. Rudolph, *Ultrashort Laser Pulse Phenomena*, II ed. (Academic, Boston, 2006).
[48] L. Mandel and E. Wolf, *Optical Coherence and Quantum Optics* (Cambridge University, Cambridge, 1995).
[49] S. A. Ponomarenko, H. Roychowdhury, and E. Wolf, "Physical significance of complete spatial coherence of optical fields," Phys. Lett. A 345, 10–12 (2005).
[50] M. I. Stockman, "Nanoplasmonics: past, present, and glimpse into future," Opt. Express 19, 22029–22106 (2011).
[51] P. N. Prasad, *Nanophotonics* (Wiley, 2004).
[52] A. Bouhelier, M. Beverslius, A. Hartschuh, and L. Novotny, "Near-field second-harmonic generation induced by local field enhancement," Phys. Rev. Lett. 90, 13903 (2003).
[53] S. I. Bozhevolny, J. Beermann, and V. Coello, "Direct observation of localized second-harmonic enhancement in random metal nanostructures," Phys. Rev. Lett. 90, 197403 (2003).
[54] M. Labardi, M. Allegrini, M. Zavelani-Rossi, D. Polli, G. Cerullo, S. D. Silvestri, and O. Sveto, "Highly efficient second-harmonic nanosource for near-field optics and microscopy," Opt. Lett. 29, 62–64 (2004).
[55] M. I. Stockman, D. G. Bergman, C. Anceau, S. Brasselet, and J. Zyss, "Enhanced second-harmonic generation by metal surfaces with nanoscale roughness: Nanoscale dephasing, depolarization, and correlations," Phys. Rev. Lett. 92, 057402 (2004).
[56] N. I. Zheludev and V. I. Emelyanov, "Phase-matched second harmonic generation from nanostructured metal surfaces," J. Opt. A. 6, 26–28 (2004).
[57] A. Liebsch, "Theory of sum frequency generation from metal surfaces," Appl. Phys. B 68, 301–304 (1999).
[58] E. M. M. van der Ham, Q. H. F. Vrehen, E. R. Eltel, V. A. Yakovlev, E. V. Alieva, L. A. Kuzik, J. E. Petrov, V. A. Sychugov, and A. F. G. van der Meer, "Giant enhancement of sum-frequency yeild by surface-plasmon excitation," J. Opt. Soc. Am. B 16, 1146–1152 (1999).
[59] A. T. Georges and N. E. Karatzas, "Optimizing the excitation of surface plasmon polaritions by difference-frequency generation on a gold surface," Phys. Rev. B 85, 155442 (2012).
[60] S. A. Ponomarenko, G. P. Agrawal, and E. Wolf, "Energy spectrum of nonstationary ensemble of pulses," Opt. Lett. 29, 394–396 (2004).

[61] W. C. Chew, *Waves and Fields in Inhomogeneous Media*, II ed. (Institute of Electrical and Electronics Engineers, New York, 1995).
[62] W. Hübner, K. H. Bennemann, and K. B¨ohmer, "Theory for the nonlinear optical response of transition metals: Polarization dependence as a fingerprint of the electronic structure at surfaces and interfaces," Phys. Rev. B 50, 17597–17605 (1994).
[63] F. X. Wang, F. J. Rodriguez, W. M. Albers, R. Ahorinta, J. E. Sipe, and M. Kauranen, "Surface and bulk contributions to the second-order nonlinear optical response of a gold film," Phys. Rev. B 80, 233402 (2009).
[64] D. Krause, C.W. Teplin, and C. T. Rogers, "Optical surface second harmonic measurements of isotropic thin-film metals: Gold, silver, copper, aluminum, and tantalum," J. Appl. Phys. 96, 3626–3634 (2004).
[65] J. A. Maytorena, W. L. Mochán, and B. S. Mendoza, "Hydrodynamic model of sum and difference frequency generation at metal surfaces," Phys. Rev. B 57, 2580-2585 (1998).
[66] S. A. Ponomarenko and E. Wolf, "Spectral anomalies in Fraunhofer diffraction," Opt. Lett. 27, 1211–1213 (2002).

APPENDIX A Analytical Analysis for Waves in the Kretschmann Configuration

The Kretschmann configuration studied in this thesis can be treated as a planarly layered media. It consists of three layers: prism, gold, and air. This inhomogeneity will create a complex situation that waves are multiply reflected and transmitted. Fortunately with the theory well developed in [25] we can readily express those waves and fields in inhomogeneous media by correctly considering the corresponding Fresnel coefficients, for both linear and nonlinear process.

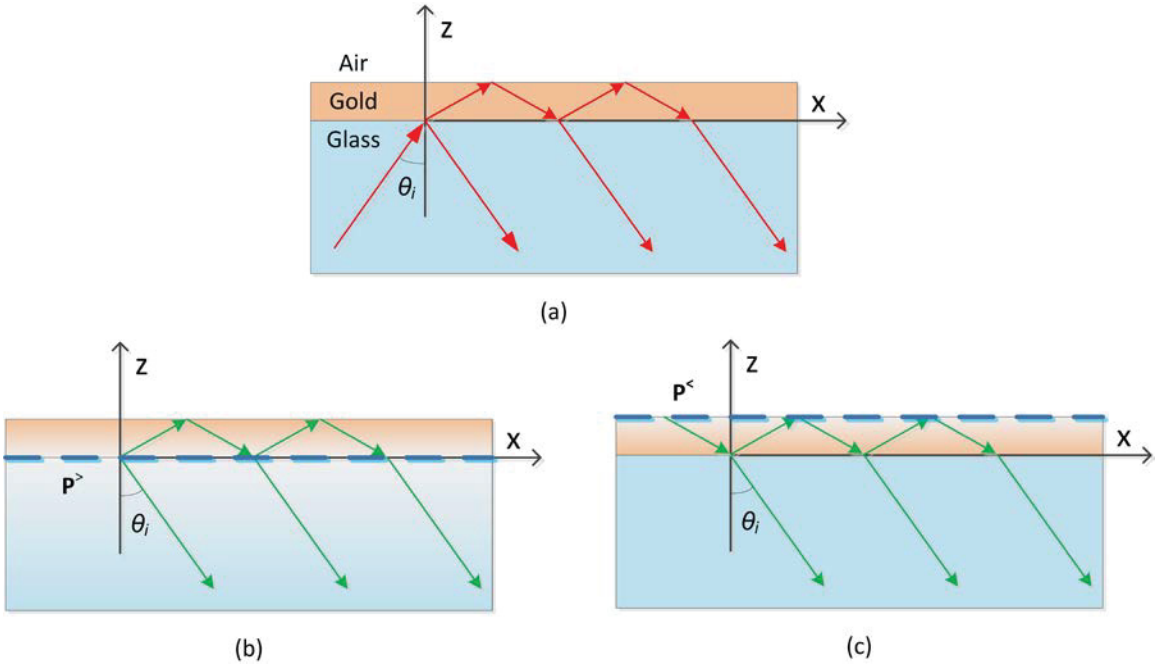

Figure A.1 Illustration of reflected FW and SFW composation. (a) The FW gets reflected by the thin film directly. Also, the total SFW in the lower half-space comes from SF polarizions at both (b) lower and (c) upper interfaces.

Seen in Fig. A.1, the incident FW at an angle of θ_i gets multiply reflected by the gold film. The wave bounces back and forth, and partially goes to the lower half-space. It can be written as

$$E_r(x,z,\omega,\theta_i) = A(\omega)(-\frac{k_{1z}}{k_1}\mathbf{e_x} - \frac{k_x}{k_1}\mathbf{e_z})\tilde{r}_{12}(\omega,\theta_i)e^{i(k_x x - k_{1z} z)}. \quad \text{(A.1)}$$

Here $\tilde{r}_{12}(\omega,\theta_i)$ is the double-interface Fresnel reflection coefficient for *p*-polarization given by [25]

$$\tilde{r}_{12}(\omega,\theta_i) = \frac{r_{12} + r_{23}e^{i2k_{2z}d}}{1 + r_{12}r_{23}e^{i2k_{2z}d}}, \quad \text{(A.2)}$$

where $k_{2z} = \sqrt{k_2^2 - k_x^2}$.

It can be shown that the total FW field in the glass is simply a superposition of the incident and reflected waves in Eqs. (2.1) and (A.1), respectively. The normal component of the reflected electric field is then

$$E_{1z}(x,z,\omega,\theta_i) = -\frac{k_x}{k_1}A(\omega)e^{ik_x x}\left[e^{ik_x x} + \tilde{r}_{12}(\omega,\theta_i)e^{-ik_{1z}z}\right]. \quad \text{(A.3)}$$

Similarly, the total FW field in the film is a superposition of the waves transmitted and reflected by the upper interface. The corresponding normal component of the field can be represented as

$$E_{2z}(x,z,\omega,\theta_i) = -\frac{k_x}{k_2}A(\omega)e^{ik_x x}\frac{t_{12}}{1 + r_{12}r_{23}e^{i2k_{2z}d}}\left[e^{ik_{2z}z} + r_{23}e^{i2k_{2z}d}e^{-ik_{2z}z}\right]. \quad \text{(A.4)}$$

The nonlinear polarization field at the lower interface $P^<$ gives rise to a contribution to the SFW through the field directly reflected into the lower half-space [Fig. A.1(b)]. It can be obtained by substituting from Eqs. (2.12) and (2.17) into Eq. (2.16), and using Eq. (2.18), yielding

$$\mathbf{E}_{down}^{(2)<}(x,z,\omega_3,\theta_i)=\frac{i\omega_3\sin\theta_i}{8\pi^2\varepsilon_0 c\sqrt{\varepsilon_1}}P_0^{<}(\omega_3,\theta_i)(-\mathbf{e_x}+\tan\theta_i\mathbf{e_z})e^{i[k_x(\omega_3)x-k_{1z}(\omega_3)z]}, \qquad (A.5)$$

where $\mathbf{k}_1(\omega_3)=k_x(\omega_3)\mathbf{e_x}+k_{1z}(\omega_3)\mathbf{e_z}$. By the same token, the other contribution from $\mathbf{P}^{<}$ to the SF field, partially transmitted into the film and eventually reflected back to the lower half-space, is

$$\mathbf{E}_{up}^{(2)<}(x,z,\omega_3,\theta_i)=\frac{i\omega_3\sin\theta_i}{8\pi^2\varepsilon_0 c\sqrt{\varepsilon_2(\omega_3)}}P_0^{<}(\omega_3,\theta_i)(-\mathbf{e_x}+\tan\theta_i\mathbf{e_z})$$
$$\times\frac{r_{23}t_{21}e^{i2k_{2z}(\omega_3)d}}{1+r_{12}r_{23}e^{i2k_{2z}(\omega_3)d}}e^{i[k_x(\omega_3)x-k_{1z}(\omega_3)z]}. \qquad (A.6)$$

The Fresnel coefficients here are all evaluated at the frequency $\omega_3=\omega_1+\omega_2$ while $k_2(\omega_3)=\sqrt{k_x^2(\omega_3)+k_{2z}^2(\omega_3)}$.

Following Fig. A.1(c), the contribution to the reflected SFW from the nonlinear polarization field at the upper interface $\mathbf{P}^{>}$ is determined as

$$\mathbf{E}^{(2)>}(x,z,\omega_3,\theta_i)=\frac{i\omega_3\sin\theta_i}{8\pi^2\varepsilon_0 c\sqrt{\varepsilon_2(\omega_3)}}P_0^{>}(\omega_3,\theta_i)(-\mathbf{e_x}+\tan\theta_i\mathbf{e_z})$$
$$\times\frac{t_{21}e^{i2k_{2z}(\omega_3)d}}{1+r_{12}r_{23}e^{i2k_{2z}(\omega_3)d}}e^{i[k_x(\omega_3)x-k_{1z}(\omega_3)z]}. \qquad (A.7)$$

APPENDIX B Numerical Codes for Solving Linear Spectral Changes

```
%*********************************************************************
%     Linear spectral changes by Surface Plasmon Resonance
%*********************************************************************
%
%     Program author: Luyu Wang
%                     Department of Electrical and Computer Engineering
%                     Dalhousie University
%                     1360 Barrington St.
%                     Halifax, NS B3J 2X4
%                     902-999-2630
%                     luyuwang@dal.ca
%
%     Date of this version:  Mar. 24, 2013
%
%*********************************************************************

clear

%*********************************************************************
%     Parameters
%*********************************************************************

cc=2.99792458e8;            %speed of light in free space
muz=4.0*pi*1.0e-7;          %permeability of free space
epsz=1.0/(cc*cc*muz);       %permittivity of free space


epsr1=2.25;                 %permittivity of glass
epsr3=1.0;                  %permittivity of air
d=52.0e-9;                  %thickness of the gold film

d_omega1=1.6e+15*0.002;
d_thetai=0.01/180.0*pi;

%*********************************************************************
%     loop1-1: angular frequency
%*********************************************************************

ii=1;
for omega1=1.3e+15:d_omega1:1.9e+15

    lambda1=2.0*pi*cc/omega1;   %wavelength
    Si(ii)=Gaussian(omega1);    %input spectrum
    epsr21=IB_FF(lambda1);      %permittivity

    k11=sqrt(epsr1)*omega1/cc;  %wave number in glass
    k21=sqrt(epsr21)*omega1/cc; %wave number in gold film
    k31=sqrt(epsr3)*omega1/cc;  %wave number in air

%*********************************************************************
%     loop1-2: incident angle
```

```
%*************************************************************************

    jj=1;
    for thetai=41.0/180.0*pi:d_thetai:48.0/180.0*pi;

        kx1=k11*sin(thetai);    %wave number components of FF
        k1z1=sqrt(k11^2-kx1^2);
        k2z1=sqrt(k21^2-kx1^2);
        k3z1=sqrt(k31^2-kx1^2);

        r121=(epsr21*k1z1-epsr1*k2z1)/(epsr21*k1z1+epsr1*k2z1);
        r231=(epsr3*k2z1-epsr21*k3z1)/(epsr3*k2z1+epsr21*k3z1);

Rs121=(r121+r231*exp(2.0*1i*k2z1*d))/(1.0+r121*r231*exp(2.0*1i*k2z1*d));
                                %Fresnel coefficients

        S1(jj,ii)=abs(Rs121^2)*Si(ii);
                                %linear spectrum wanted

        jj=jj+1;
    end

%*************************************************************************
%     End varible loop
%*************************************************************************

    ii=ii+1;
end

%intensity normalization
for mm=1:jj-1
    S1n(mm,:)=S1(mm,:)/max(S1(mm,:));
end

mesh(S1n)
```

APPENDIX C Numerical Codes for Solving Nonlinear Spectral Changes

```
%*********************************************************************
%     Nonlinear spectrum caculated using polychromatic plane wave
%*********************************************************************
%
%     Program author: Luyu Wang
%                     Department of Electrical and Computer Engineering
%                     Dalhousie University
%                     1360 Barrington St.
%                     Halifax, NS B3J 2X4
%                     902-999-2630
%                     luyuwang@dal.ca
%
%     Date of this version:  Mar. 24, 2013
%
%*********************************************************************

clear

%*********************************************************************
%     Parameters
%*********************************************************************

cc=2.99792458e8;            %speed of light in free space
muz=4.0*pi*1.0e-7;          %permeability of free space
epsz=1.0/(cc*cc*muz);       %permittivity of free space

epsr1=2.25;                 %permittivity of glass
epsr3=1.0;                  %permittivity of air
E0=1.0;                     %input field amplitude
d=52.0e-9;                  %thickness of the gold film

d_omega1=1.6e+15*0.01;
d_omega2=3.2e+15*0.01;
d_thetai=0.1/180.0*pi;

%*********************************************************************
%     loop 1: SH angular frequency
%*********************************************************************

ii=1;
for omega2=2.6e+15:d_omega2:3.8e+15

    lambda2=2.0*pi*cc/omega2;   %wavelength

    epsr22=IB_SH(lambda2);      %permittivity
    e_3=LD(lambda2,'Au','D');   %permittivity for kai caculation -
Drude

    k12=sqrt(epsr1)*omega2/cc;  %wave number in glass
    k22=sqrt(epsr22)*omega2/cc; %wave number in gold film
    k32=sqrt(epsr3)*omega2/cc;  %wave number in air
```

```
%**********************************************************************
%     loop 1.1: incident angle
%**********************************************************************

    jj=1;
    for thetai=0.0/180.0*pi:d_thetai:90.0/180.0*pi;

        kx2=k12*sin(thetai);    %wave number components of SH
        k1z2=sqrt(k12^2-kx2^2);
        k2z2=sqrt(k22^2-kx2^2);
        k3z2=sqrt(k32^2-kx2^2);

%**********************************************************************
%     loop 1.2: FF angular frequency
%**********************************************************************

        sum1=0.0;                               %for integral caculation
        sum2=0.0;

        kk=1;
        for omega1=0.6e+15:d_omega1:2.6e+15

            [F1_w1,F2_w1,A1(kk),epsr2_w1,e_1]=Fresnel(omega1,thetai);

            omega11=omega2-omega1;

            [F1_w2,F2_w2,A2(kk),epsr2_w2,e_2]=Fresnel(omega11,thetai);

            %intergral caculation
            kai=kai_zzz(e_1,e_2,e_3);

            I1=kai*F1_w1*A1(kk)/epsr2_w1*F1_w2*A2(kk)/epsr2_w2*d_omega1;
            I2=kai*F2_w1*A1(kk)*F2_w2*A2(kk)*d_omega1;

            sum1=sum1+I1;
            sum2=sum2+I2;

            kk=kk+1;
        end

        Il=sum1;
        Iu=sum2;

        p0lz=epsz*epsr1^2*sin(thetai)^2*Il/2.0/pi;     %lower interface
        p0uz=epsz*sin(thetai)^2*Iu/2.0/pi;             %upper interface


        %Fresnel coefficient at SH frequencies
        r122=(epsr22*k1z2-epsr1*k2z2)/(epsr22*k1z2+epsr1*k2z2);
        r232=(epsr3*k2z2-epsr22*k3z2)/(epsr3*k2z2+epsr22*k3z2);
        t212=2.0*sqrt(epsr1*epsr22)*k2z2/(epsr1*k2z2+epsr22*k1z2);
```

```
frsl=r232*t212*exp(2.0*1i*k2z2*d)/(1.0+r122*r232*exp(2.0*1i*k2z2*d));
        frsu=t212*exp(1i*k2z2*d)/(1.0+r122*r232*exp(2.0*1i*k2z2*d));


        %field caculation

Exld=1i*p0lz*omega2/cc*E0^2*sin(thetai)/8.0/pi^2/epsz/sqrt(epsr1);

Ezld=1i*p0lz*omega2/cc*E0^2*sin(thetai)^2/8.0/pi^2/epsz/sqrt(epsr1)/cos
(thetai);

Exlu=1i*p0lz*omega2/cc*E0^2*sin(thetai)/8.0/pi^2/epsz/sqrt(epsr22)*frsl;

Ezlu=1i*p0lz*omega2/cc*E0^2*sin(thetai)^2/8.0/pi^2/epsz/sqrt(epsr22)/co
s(thetai)*frsl;

Exu=1i*p0uz*omega2/cc*E0^2*sin(thetai)/8.0/pi^2/epsz/sqrt(epsr22)*frsu;

Ezu=1i*p0uz*omega2/cc*E0^2*sin(thetai)^2/8.0/pi^2/epsz/sqrt(epsr22)/cos
(thetai)*frsu;


        %intensity caculation
        Ex=Exld+Exlu+Exu;
        Ez=Ezld+Ezlu+Ezu;
        S2(jj,ii)=abs(Ex^2+Ez^2);

        jj=jj+1;
    end

%**************************************************************************
%     End varible loop
%**************************************************************************

    ii=ii+1;
end

%intensity normalization
for mm=1:jj-1
    S2n(mm,:)=S2(mm,:)/max(S2(mm,:));
end

mesh(S2n)
```

APPENDIX D Copyright Permission

From: Luyu Wang [mailto: ly737715@dal.ca]
Sent: Thursday, July 04, 2013 3:14 PM
To: pubscopyright
Subject: Permission

Dear Optical Society of America,

I am the first author of the following journal, while I was working towards my master degree. Now, I am preparing my master thesis for submission to the Falcuty of Graduate Studies at Dalhousie University, Halifax, Nova Scotia, Canada. I am seeking your permission to include a manuscript version of the following paper as a chapter in the thesis:

Luyu Wang, Franklin Che, Sergey A. Ponomarenko, and Zhizhang (David) Chen, "Plasmon-enhanced spectral changes in surface sum-frequency generation with polychromatic light", Opt. Express, 21, 14159 (2013).

Full publication details and a copy of this permission letter will be included in the thesis.

Best Regards,

Luyu Wang

Date: Tue, 9 Jul 2013 16:34:43 +0000 [07/09/13 1:34:43 PM ADT]
From: pubscopyright <copyright@osa.org>
To: Luyu Wang <ly737715@dal.ca>
Subject: RE: Permission

Dear Luyu Wang,

Thank you for contacting The Optical Society.

Because you are the author of the source paper from which you wish to reproduce material, OSA considers your requested use of its copyrighted materials to be permissible within the author rights grated in the Copyright Transfer Agreement submitted by the requester on acceptance for publication of his/her manuscript. It is requested that a complete citation of the original material be included in any publication. This permission assumes that the material was not reproduced from another source when published in the original publication.

Please let me know if you have any questions.

Kind Regards,

Susannah Lehman

Susannah Lehman
July 9, 2013
Authorized Agent, The Optical Society